CDK4 and CDK6 upregulation promotes DNA replication stress, genomic instability and resistance to EGFR targeted therapy in lung cancer

Beatrice Gini[1,2], Philippe Gui[1,2], Wei Wu[1,2], D. Lucas Kerr[1,2], Lisa Tan[1,2], Dora Barbosa[1,2], Victor Olivas[1,2], Carlos Gomez[1,2], Sarah Elmes[2], Veronica Steri[2], Turja Chakrabarti[1,2], Trever G. Bivona[1,2,3] *, Collin M. Blakely[1,2] *

Author Affiliations

1 Department of Medicine, University of California, San Francisco, San Francisco, CA 94158, USA.

2 Helen Diller Family Comprehensive Cancer Center, University of California, San Francisco, San Francisco, CA 94158, USA.

3 Chan-Zuckerberg Biohub, San Francisco, CA 94158, USA.

*co-corresponding authors

Email: collin.blakely@ucsf.edu or trever.bivona@ucsf.edu

Abstract

Genetic interactions impact both normal human physiology and human diseases, such as cancer. Here, we study genetic interactions through the lens of human lung cancers driven by oncogenic forms of the epidermal growth factor receptor (EGFR), which we and others previously showed harbor a rich landscape of genetic co-alterations and potential genetic interactions. Among the most common genetic co-alterations with oncogenic *EGFR* are genomic amplifications of cell cycle regulators *CDK4* or *CDK6*, which have been implicated in EGFR inhibitor clinical resistance, although the mechanism underlying this effect is not well characterized. We show that CDK4/6 upregulation overcomes EGFR inhibitor-induced G1/S cell cycle arrest in association with increased replication stress, DNA damage and genomic instability. These biological effects arising in CDK4/6 upregulated tumors help to enable resistance to EGFR targeted therapies through established genetic resistance mechanisms. Combinatorial EGFR and CDK4/6 inhibitor treatment alleviated genomic instability and EGFR inhibitor resistance in patient-derived preclinical models. This study reveals mechanistic and clinical impacts of the genetic interaction between oncogenic *EGFR* and *CDK4/6* co-alterations in human lung cancer.

Main Text

Understanding how genetic interactions regulate physiologic and pathologic cell biology can shed light on the mechanisms governing cellular behaviors, including cell metabolism, proliferation, and apoptosis[1,2], with therapeutic implications[3]. Such genetic interactions can contribute to ultimate cell and tissue phenotypes as well as phenotypic heterogeneity and plasticity[1-3]. Many diseases including cancer arise not just via single gene aberrations but also

2

through multiple complex genetic events[4]. The extent to which, and mechanisms by which genetic interactions promote cancer and its associated phenotypes is important and incompletely understood. Further characterization of these genetic interactions will allow us to more completely define disease pathogenesis and identify improved treatment strategies.

We sought a deeper understanding of somatic genetic interactions affecting the pathogenesis and treatment of non-small cell lung cancer (NSCLC), which accounts for approximately 85% of lung cancers and is the leading cause of cancer-related mortality worldwide[5,6]. Among NSCLC, lung adenocarcinoma (LUAD) is the most common histologic subtype[7]. Targetable oncogenic driver mutations are now identifiable in the majority of LUAD cases[8]. Oncogenic activating mutations in epidermal growth factor receptor (EGFRmt) are present in ~ 15-30% of patients in the U.S. and more than 50% of cases in Asia[9-11]. Small molecule EGFR tyrosine kinase inhibitors (TKIs), including erlotinib, gefitinib, afatinib, dacomitinib, and the third generation EGFR inhibitor osimertinib improve overall response (ORR) rate as well as progression-free survival (PFS) compared to traditional cytotoxic chemotherapy. However, TKI-resistance limits the effectiveness of these therapies after approximately one to three years for patients with metastatic disease[12-14]. Several mechanisms of acquired resistance to EGFR TKIs have been identified, including on-target mutations within *EGFR*, amplification of other receptor tyrosine kinases (RTKs), such as *MET*, oncogenic fusions involving *ALK* and *RET*, as well as activating mutations within the MAPK signaling pathway[15]. A role for genes known to regulate cell cycle progression, including *CDK4* and *CDK6,* has also emerged as potential resistance mechanisms[3,16,17].

Interrogation of the genomic alteration landscape present in circulating tumor DNA (ctDNA) from 1,122 advanced stage *EGFR* mutant NSCLC patients previously allowed us to

uncover genetic co-alterations beyond oncogenic EGFR which could potentially impact response to EGFR targeted therapies[3]. Among the most common genetic co-alterations identified were alterations in cell cycle regulatory genes, which were clinically associated with decreased response to osimertinib, as well as reduced PFS and overall survival (OS) in advanced EGFR-mutant lung adenocarcinoma cases[3]. Importantly, these cell cycle gene alterations were also associated with acquired resistance to osimertinib, but the mechanism by which they promote EGFR TKI resistance was unclear[3]. Among the cell cycle regulatory genes, *CDK4* and *CDK6* copy number alterations (CNAs) were most closely associated with decreased PFS and resistance upon osimertinib treatment[3]. Recent clinical data further support a role for *CDK4* and *CDK6* gene alterations in de novo EGFR TKI resistance in *EGFR* mutant NSCLC patients[17]. CDK4 and CDK6 proteins regulate G1/S cell cycle progression through phosphorylation of retinoblastoma protein 1 (RB1). Phosphorylation of RB1 releases its inhibitory binding to transcription factor family E2F which mediates the transition from G1 to S-phase of the cell cycle[18].

Alterations in cell cycle genes have been shown to induce significant deregulation of cell cycle checkpoints, compromising DNA integrity, and contribute to the accumulation of DNA damage and abnormal chromosomal segregation[19-21]. The extent to which each cell cycle gene alteration affects DNA stability and integrity and the implications for cancer therapy are currently unknown. Here, we investigated the mechanistic roles and potential clinical impacts of concurrent alterations in cell cycle genes more generally and *CDK4/6* CNAs specifically in EGFR-mt LUAD, with potentially important therapeutic implications.

Results

CDK4/6 **CNAs are associated with significantly increased genomic instability in EGFRmt LUAD patient tumors.**

To determine the impact of cell cycle gene alterations on EGFRmt NSCLC genomic stability, with a focus on *CDK4/6* CNAs, we analyzed targeted exome sequencing datasets from a cohort of 660 EGFRmt advanced NSCLC cases profiled by Foundation Medicine (FM) with a panel of 401 cancer-relevant genes. These clinical cases were divided into two cohorts: those bearing alterations in any of the cell cycle genes defined by TCGA[22], and cases negative for such alterations (Fig. 1a,b). In the cell cycle altered cohort, the most common cell cycle gene alterations were in the tumor suppressor genes *CDKN2A/2B* (49%-38.7%), and *Rb1* (21.8%) (Fig. 1a). *CDK4* (15.7%), CCNE1 (10%), CCND1 (8%) and *CDK6* (6.7%) alterations were the next most common cell cycle altered genes (Fig. 1a). *CDK4* and *CDK6* alterations were predominantly copy-number gains that were mutually exclusive from one another and with a higher frequency of representation in EGFRmt LUAD compared to LUAD cases with wild type EGFR (Fig. 1a and Supplementary Fig. 1a). Alterations in *TP53*, which could indirectly regulate cell cycle progression, were similarly represented across the two patient cohorts (68% of positive and 63% of negative patients; Fig. 1a,b). As a measure of genomic instability (GIN), we assessed the fraction of genome alterations (FGA)[23] and tumor mutational burden (TMB)[24]. EGFRmt NSCLC cases with concurrent cell cycle gene alterations demonstrated a significantly increased FGA and TMB compared to the negative cohort (Fig. 1c and Supplementary Fig. 1b). A significant increase in FGA and TMB in EGFRmt cell cycle gene alteration positive cases were also found in the MSK-IMPACT NSCLC dataset, which includes 95% LUAD cases (Fig. 1d and Supplementary Fig. 1c).

5

To determine the extent to which individual cell cycle genes contribute to GIN, we assessed the impact of specific cell cycle gene alterations on tumor FGA in FM and MSK-IMPACT datasets. Tumors with *CDK4* or *CDK6* CNAs demonstrated a significant increase in FGA (Fig. 1e,f), but not in TMB (Supplementary Fig. 1d,e). Tumors that harbored *RB1* alterations showed similar FGA increased to *CDK4/6* CNAs positive tumors (Supplementary Fig. 1f), whereas *CCND1* or *CCND3* alterations showed a minimal increase in FGA (Supplementary Fig. 1g,h). In contrast, tumors with alterations in *CDKN2A*, *CDKN2B*, or *CCNE1* demonstrated no difference in FGA (Supplementary Fig. 1i-k). FGA was also found to be positively correlated with the degree of *CDK4/6* copy number gain in the FM dataset (Fig.1g).

To determine whether increased FGA is associated with other commonly amplified genes in EGFRmt NSCLC, we assessed FGA in tumors with amplifications in *NFKBIA* (amplified in 18% of cases), the most frequent gene amplification in this cohort and that is not known to be directly involved in cell cycle regulation, and in *MDM2* (amplified in 14% of cases), the most frequent gene amplification in this cohort and that is indirectly associated with G1/S checkpoint regulation, compared to the FGA of non-amplified tumors. We found no significant difference among these subgroups (Supplementary Fig. 2a,b), suggesting that increased FGA is more common in tumors with cell cycle gene alterations. Next, we analyzed whether *CDK4/6* CNAs are associated with whole genome doubling (WGD), an additional indicator of GIN[25]. As WGD analysis is enabled by whole exome sequencing (WES), we analyzed the TCGA NSCLC dataset and found a significantly higher number of WGD positive cases in the presence of *CDK4/6* CNAs (Fig. 1h).

Overall, these data suggest that of the co-occurring cell cycle gene alterations in EGFR-mutated NSCLC, *CDK4/6* CNAs and *RB1* alterations are most associated with decreased genomic

integrity in EGFRmt lung cancers. The impact of *RB1* alterations on EGFR inhibitor resistance has been extensively characterized[26,27]. *RB1* alterations are only represented in a small percentage of *CDK4/6* CNAs positive cases (Supplementary Fig. 2c,d), prompting us to investigate the potential role and underlying mechanisms of *CDK4/6* CNAs in EGFR targeted therapy resistance in EGFRmt NSCLC.

***CDK4/6* overexpression or amplification increases genomic instability in EGFRmt LUAD CDX and PDX models.**

Given the increase in GIN observed in EGFRmt NSCLC cases with *CDK4/6* CNAs, we tested whether *CDK4* or *CDK6* amplification or overexpression may cause increased genomic instability (GIN) in preclinical models. As a measure of GIN, we assessed the FGA in EGFRmt LUAD CDXs and primary, patient derived PDXs and PDOs. We observed a 20-fold increase in FGA in CDK4 and CDK6 overexpressing EGFRmt NSCLC tumor xenografts compared to EV controls (Fig. 2a and Supplementary Fig. 3a) and a 2-fold increase in FGA in *CDK6* amplified TH116 and TH21 EGFRmt PDXs compared to patient derived TH107, *CDK4/6* non-amplified, EGFRmt organoids (Supplementary Fig. 3b-h). We performed single-cell resolution, karyotypic characterization assays of CDK4/6 overexpressing H1975 CDXs using DNA content analysis by flow cytometry. A higher percentage of cells from CDK4 or CDK6 overexpressing H1975 CDXs were found to have > 2N DNA content compared to EV controls (Fig. 2b), indicating a higher degree of aneuploidy. CDK4 or CDK6 overexpressing CDXs also exhibited a significantly higher percentage of cells undergoing mitosis, as demonstrated by immunofluorescence staining for the centrosome marker γ-tubulin (Fig. 2c-e). Pan-centromere FISH (Supplementary Fig. 4a-c) analysis of FFPE tumor tissues confirmed a higher degree of aneuploidy in CDK4 or CDK6 overexpressing CDXs (Supplementary Fig. 4d-e).

These collective data suggest that CDK4 or CDK6 upregulation induces an accumulation of chromosomal aberrations in EGFRmt NSCLC xenografts and that, despite this, a subset of cells retain the capacity to undergo mitosis.

CDK4/6 upregulation bypasses the G1/S checkpoint leading to premature DNA synthesis in EGFRmt LUAD.

To identify the mechanism by which CDK4/6 overexpression promotes GIN, we assessed gene expression changes induced by CDK4/6 overexpression in CDXs. Gene set enrichment analysis of CDK4 or CDK6 overexpressing H1975 tumor xenografts showed significant upregulation of E2F1 target genes, which mediate G1/S transition, together with significant enrichment of G2/M checkpoint, DNA repair genes and downregulation of epithelial-to-mesenchymal transition (EMT), NFκB, p53, and apoptosis pathways (Fig. 3a and Supplementary Fig. 5a-c). These data suggest that NSCLC tumors overexpressing CDK4 or CDK6 may bypass the G1/S checkpoint, leading to pre-mature DNA synthesis while also exhibiting CDK4/6-associated changes in lineage state and inflammatory and apoptotic programs.

We tested this hypothesis by assessing the quantity of newly synthesized DNA through measurement of EdU incorporation in CDK4 and CDK6 overexpressing tumor xenografts compared to EV controls. Immunofluorescence analysis of EdU incorporation in CDK4 and CDK6 overexpressing H1975 CDXs demonstrated a significant increase in DNA synthesis compared to EV controls (Fig. 3b,c). This was consistent with the higher Ki67 positivity in the CDK4/6 overexpressing tumor xenografts versus controls (Supplementary Fig. 6a,b). Upon EGFR TKI treatment, CDK4/6 overexpressing CDXs retained higher DNA synthesis compared to controls (Fig. 3b,d). Furthermore, there were increased levels of Retinoblastoma-associated protein

8

phosphorylation (p-Rb) and of the cell cycle gene cyclin E1 (CCNE1) during osimertinib treatment in CDK6 overexpressing HCC827 and H1975 EGFRmt NSCLC cells compared to controls (Fig. 3e,f), suggesting that CDK6 overexpression is sufficient to overcome the G1/S arrest associated with osimertinib treatment. G1/S progression was further characterized using a FUCCI dual sensor assay[28]. There was a significantly higher percentage of cells in S/G2/M phases in HCC827 CDK6 expressing 3D colonies versus control cells, both pre- and post-treatment with EGFR TKI (Supplementary Fig. 6c,d). Taken together, these data demonstrate that overexpression of CDK4 or CDK6 results in enhanced entry into S phase of the cell cycle that is maintained during osimertinib treatment.

CDK4/6 upregulation bypasses the G1/S checkpoint leading to replication stress in EGFRmt LUAD.

Given that the G1/S checkpoint of the cell cycle is necessary to ensure cellular repair of DNA damage prior to DNA replication[29], we hypothesized that CDK4/6 overexpression would lead to an accumulation of intracellular DNA damage. We tested this hypothesis using double immunofluorescence staining for gamma-H2AX and EdU in H1975 CDK4 and CDK6 overexpressing tumor xenografts (Fig. 4a,b). Specifically, we quantified gamma-H2AX foci in proliferating, EdU positive cells, as a measure of double-strand DNA breaks (Fig. 4c). H1975 CDK4 and CDK6 overexpressing CDXs showed significantly higher gamma-H2AX foci in proliferating cells than controls (Fig. 4a,c). This effect persisted during osimertinib treatment (Fig. 4b,c and Supplementary Fig. 7a).

Next, we tested whether the accumulation of DNA damage could be a consequence of additional replication stress caused by premature DNA synthesis entry in CDK4/6 overexpressing

NSCLC tumors. We evaluated the level of a panel of biomarkers indicative of DNA replication stress using immunoblotting[30,31]. The protein panel included: phosphorylation of Retinoblastoma-associated protein (Rb1), TPX2 microtubule nucleation factor (TPX2), phosphorylation of replication protein A (RPA), as well as phosphorylation of ataxia-telangiectasia mutated (ATM). H1975 and PC9 CDK4 and CDK6 expressing CDXs demonstrated significantly higher expression levels of replication stress biomarkers compared to EV controls (Fig. 4d,e and Supplementary Fig. 7b). Given the role of TPX2 during interphase as a protecting factor of DNA fork stability during replication stress[31], we assessed nuclear expression of TPX2 in CDK4 and CDK6 overexpressing CDXs by immunohistochemistry and identified increased TPX2 nuclear expression compared to EV controls (Fig. 4f,g). Increased TPX2 nuclear localization in H1975 CDK4 and CDK6 overexpressing CDXs was also observed post-osimertinib treatment, although it was decreased compared with pre-treatment levels (Fig. 4f,g). *TPX2* gene expression has been shown to depend on the activity of transcription factor E2F1[32,33], which is in line with the downregulation of the *TPX2* gene that we observed upon transient E2F1 knockdown (Supplementary Fig. 7c,d). CDK4 and CDK6 overexpressing CDXs also demonstrated increased expression of phosphorylated ATM (Fig. 4d,e), indicative of DNA damage response (DDR) activation. Further analysis of RNA sequencing data obtained from CDK4/6 overexpressing H1975 CDXs revealed evidence of upregulation of key DDR inducers and effectors, including CHEK1, CHEK2, RAD51 and BRCA1, supporting this hypothesis (Supplementary Fig. 7e).

CDK4/6 overexpression induces resistance to EGFR targeted therapy and acquisition of secondary oncogenic alterations in EGFRmt LUAD.

To better understand the effects of *CDK4* or *CDK6* CNAs induced GIN on EGFRmt lung cancer cell responsiveness to EGFR TKI treatment we assessed a panel of EGFRmt NSCLC cell lines (H1975, PC9, HCC827) and primary, patient-derived organoid (PDO) cultures from an EGFR Exon 19 deletion positive NSCLC patient (TH107) (Supplementary Table 1-2). CDK4 or CDK6 overexpression in NSCLC cells (Supplementary Figs. 3a and 8a and Supplementary Table 2) conferred relative resistance to osimertinib treatment compared to control cells in long-term 2D assays (Supplementary Fig. 8b) and 3D cultures (Fig. 5a-c and Supplementary Fig. 8c-h), indicating that CDK4 or CDK6 upregulation induces osimertinib resistance. TH107 PDOs, which had no evidence of *CDK4* or *CDK6* CNAs (Supplementary Fig.3f,g), were genetically engineered to overexpress CDK4 or CDK6 through lentiviral infection to model *CDK4/6* CNAs (Supplementary Fig.9a and Supplementary Table 1-2).[34] CDK4/6 overexpressing TH107 PDOs were resistant to EGFR inhibitor (osimertinib) treatment in a 35-day assay (Fig. 5d,e and Supplementary Fig.9b,c).

To test whether CDK4 or CDK6 upregulation affects response to EGFR TKI treatment *in vivo*, we compared the TKI sensitivity of CDK4/6 overexpressing H1975 and PC9 CDXs to empty vector (EV) controls (Supplementary Table 2). First, we observed significantly increased tumor volumes in vehicle-treated CDK6 overexpressing H1975 and PC9 CDXs compared to controls (Supplementary Fig. 10a,b), suggesting that CDK6 overexpressing tumors have a higher growth potential. We next assessed the osimertinib sensitivity of H1975 CDXs across a dose range from 2.5 mg/kg/day to 10 mg/kg/day and found that 5 mg/kg/day was sufficient to inhibit EGFR phosphorylation and signaling in these models (Fig. 5f). Osimertinib treatment suppressed the

11

growth of H1975-EV xenografts, whereas CDK4 or CDK6 overexpressing tumor xenografts showed osimertinib resistance (Fig. 5g,h, Supplementary Fig. 10c).

We classified the change in tumor volume under treatment using criteria in alignment with RECIST 1.1, which include complete response (CR), partial response (PR) being defined a decrease in tumor volume by at least 30%, progressive disease (PD) being defined as an increase in tumor volume by at least 20%, and stable disease (SD) between -30% and + 20%[35]. All EGFR L858R, T790M H1975 CDK6 overexpressing tumors (5/5) exhibited PD, whereas no E.V. control tumors met criteria for PD (Supplementary Fig. 10d-f and Supplementary Table 3). To determine whether these results were generalizable to other EGFRmt lung cancer models, we tested *EGFR*Del19 PC9 CDXs overexpressing CDK6 or EV control that were treated with osimertinib (Supplementary Fig. 11a and Supplementary Table 3). PC9 CDXs overexpressing CDK6 similarly exhibited osimertinib resistance compared to EV controls (Supplementary Fig. 11a-c), with higher degrees of CDK6 expression in tumors at PD versus PR and SD (Supplementary Fig. 11d,e). Overall, these results demonstrate that CDK4 or CDK6 upregulation induces resistance to EGFR inhibitor (osimertinib) treatment in multiple EGFRmt NSCLC models.

Next, to understand the role that CDK4/6 induced GIN exerts on EGFR targeted therapy sensitivity, we assessed the degree of CNVs and non-synonymous SNVs acquisition upon osimertinib treatment in CDK4 or CDK6 overexpressing EGFRmt tumor xenografts. CDK4 or CDK6 overexpression induced significant karyotypic aberrations in the genome of osimertinib treated tumors compared to empty vector control (Supplementary Fig. 12a-c). This was accompanied by the acquisition of secondary oncogene and pathway alterations with relevant roles in EGFR TKI resistance (Supplementary Fig. 12d-e)[15,36,37]. Key genes contributing to EGFR inhibitor resistance identified were included in large scale[38] (~ 50-100 Mb) copy number gains in

12

chromosome 7 in all CDK4/6 overexpressing EGFR-mt tumors, and including *EGFR*, *MET*, *BRAF* and *CDK6* (Supplementary Fig. 12c) genes which can each (and together) induce EGFR TKI resistance.[15] *EGFR* gene chromosomal gain co-localized with gain in *CDK6* gene in one sample, whereas *MET* and *BRAF* gene chromosomal gains were detected and co-localized in 3 out of 4 tumors, two of which also included gain in *CDK6* gene (Supplementary Fig. 12c). These secondary gene alterations were also among the most frequent present in clinical cases carrying concurrent *EGFR* mutations and *CDK4* or *CDK6* amplification in a cBioPortal cross-analysis (Supplementary Fig. 13a-c). Compared to vehicle treated tumors, osimertinib induced significant acquisition of unique, non-synonymous SNVs in all xenografts, regardless of CDK4/6 status (Supplementary Fig. 12d), with no significant differences in TMB, consistent with our clinical data (Supplementary Fig. 1d-e). In line with these results, previous data reported increased DNA damage[39] and enhanced APOBEC activity[40] in LUAD tumors following EGFR TKI treatment, both of which could contribute to the accumulation of SNVs that we observed. In order to check whether, despite the general increase in TMB in all tumors, CDK4/6 upregulation triggers enrichment of SNVs belonging to specific TCGA-defined oncogenic pathways[22], we performed pathway analysis of SNVs uniquely represented in CDK4/6 overexpressing EGFRmt tumor xenografts, with predicted functional impact. This analysis revealed previously recognized EGFR TKI resistance processes including TGF-β, NRF2, RTK/RAS and WNT signaling as the most enriched in these tumors (Supplementary Fig. 12e)[41-43]. Taken together, CNVs and SNVs analyses highlighted the presence of a subset of alterations associated with EGFR TKI resistance in CDK4 or CDK6 upregulated EGFRmt LUAD tumors.

Combination therapy with oncogenic EGFR (osimertinib) and CDK4/6 inhibitors decreases replication stress and genomic instability in EGFRmt LUAD models, reduces cell proliferation, and enhances apoptosis.

We hypothesized that inhibition of CDK4/6 activity may decrease tumor cell proliferation, and subsequent replication stress (RS) and restore osimertinib sensitivity in CDK4/6-upregulated EGFRmt LUAD models. We treated EGFRmt, CDK4/6 overexpressing H1975 CDXs with the FDA-approved CDK4/6 inhibitor palbociclib in combination with osimertinib (Fig. 6a and Supplementary Table 2). Combinatorial therapy more potently suppressed growth of CDK4/6-upregulated CDX models than osimertinib or palbociclib monotherapy, significantly decreasing tumor sizes (Fig. 6a,b, Supplementary Fig.14a). The response to combination therapy with osimertinib plus palbociclib was durable when we extended the treatment to 35 days, showing significant tumor regression (Supplementary Fig. 14b). Tumors regrew only upon treatment cessation (Supplementary Fig. 14b). These data indicate that the addition of a CDK4/6 inhibitor to EGFR TKI treatment can overcome EGFR TKI resistance associated with CDK4/6 upregulation.

To test whether the increased sensitivity to combinatorial treatment of CDK4/6 overexpressing CDXs was linked to downregulation of RS and DNA damage, we assessed nuclear expression of p-Rb, p-RPA and gamma-H2AX by immunohistochemistry in CDK4 overexpressing H1975 CDXs. Combination treatment with osimertinib and palbociclib more significantly reduced the percentage of CDK4 and p-Rb positive nuclei compared to monotherapy with osimertinib or palbociclib (Fig. 6c-f and Supplementary Fig. 14c,d). Moreover, combination therapy more effectively suppressed p-RPA, gamma-H2AX positive nuclei (Fig. 6g-j) and induced a higher degree of tumor necrosis (Fig. 6k,l and Supplementary Fig. 14e). Overall, these results highlight a more effective inhibition of G1/S progression and DNA damage accumulation, with

14

enhanced cell death, in CDK4/6 overexpressing CDXs using combination of EGFR and CDK4/6 inhibitors.

To further assess the translational relevance of our findings, we performed preclinical trials using PDOs and PDXs. EGFR Del19 TH107 CDK6 overexpressing PDOs were used to test monotherapy and combination treatment with osimertinib and the CDK4/6 inhibitor abemaciclib (Supplementary Table 1-2). Combinatorial treatment enhanced sensitivity to osimertinib in the otherwise resistant CDK4/6 upregulated models (Supplementary Fig. 14f).

The effect of combination with osimertinib plus palbociclib therapy was also assessed in a PDX tumor model (TH-116), developed from a LUAD biopsy at resistance to osimertinib treatment, which harbored a concurrent EGFR L858R mutation and *CDK6* CNA (Supplementary Fig. 3b,c and Supplementary Table 1-2). This tumor also exhibits elevated FGA compared to a non-*CDK6* amplified EGFRmt PDX (Supplementary Fig 3h). In this primary, patient-derived model we determined that osimertinib 5 mg/kg and palbociclib 150 mg/kg were sufficient to block EGFR and CDK4/6 activation, respectively (Fig. 7a). TH116 PDXs continued to grow during osimertinib treatment indicating EGFR TKI resistance (Fig. 7b,c, Supplementary Fig. 15a and Supplementary Table 3). However, tumor growth was significantly diminished by the addition of the CDK4/6 inhibitor palbociclib with no overt signs of substantial toxicity (Fig. 7c,d, Supplementary Fig. 15a and Supplementary Table 3). To evaluate whether palbociclib plus osimertinib co-treatment could impact RS and GIN, we assessed tumor gamma-H2AX expression (Fig. 7e,f) and FGA (Fig. 7g). Tumor gamma-H2AX protein expression was significantly reduced with palbociclib in monotherapy and combination therapy with osimertinib, without showing significant changes in the CDK6 protein expression (Fig. 7e,f and Supplementary Fig. 15b-d). A significant reduction of FGA compared to vehicle treated tumors was observed only when

osimertinib was combined with palbociclib (Fig. 7g). The data suggest that blocking the activity of CDK4/6 alleviates DNA damage, leading to diminished tumor GIN in primary, patient-derived in vivo NSCLC models.

Next, we investigated whether the significant reduction of RS and GIN detected in tumors treated with combinatorial osimertinib plus palbociclib was concurrent with a more effective suppression of tumor proliferation and induction of apoptosis. We assessed nuclear expression of Ki67 and cleaved caspase 3 by immunohistochemistry as a measure of proliferation and apoptosis, respectively, in empty vector control and CDK4/6 overexpressing EGFRmt tumors treated with EGFR TKI (osimertinib) under monotherapy and combinatorial therapy (Fig. 8a-b). We observed significant suppression of Ki67 levels and increased cleaved caspase 3 in CDK4/6 overexpressing tumors specifically under the combinatorial treatment (Fig. 8c-d). These data suggest that concurrent inhibition of EGFR and CDK4/6 can significantly suppress tumor proliferation and induce apoptosis in CDK4/6 upregulated LUAD tumors.

Discussion

Overall, this study sheds light on the mechanistic role of complex somatic genetic interactions in mammalian cells that drive disease pathogenesis and cancer therapy resistance. The findings provide strong rationale to study genetic interactions and their functional and therapeutic relevance more deeply in human cancers. Our work highlights the clinical and functional significance of co-occurring tumor genomic alterations in oncogene-driven NSCLC, which are generally poorly understood in NSCLC and other cancer types. We demonstrate that *CDK4* and *CDK6* amplification are associated with increased FGA in EGFRmt lung cancers in multiple

16

clinical datasets. Increased FGA has been shown to associate with poor prognosis in patients with early-stage NSCLC[23]. Similarly, in the TRACERx study, increased copy number heterogeneity was associated with GIN and increased risk of recurrence or death in patients with NSCLC[44,45]. In our analysis of two large independent patient cohorts, approximately 50% of EGFRmt NSCLCs harbor concurrent alterations of cell cycle related genes, with *CDK4* or *CDK6* amplification observed in approximately 10% of tumors. Evidence of increased FGA with *CDK4/6* CNAs was present in both cohorts, suggesting that CDK4/6 upregulation may play a role in promoting GIN and poor outcomes in EGFRmt NSCLC.

We found that replication stress and genomic instability in EGFRmt tumors contribute to therapy resistance. Activating EGFR mutations, such as L858R or exon 19 deletions, drive constitutive signaling through the MAPK pathway, culminating in ERK phosphorylation and activation of transcription factors that promote G1/S cell cycle progression[46]. Osimertinib and other EGFR TKIs induce cell cycle G1 arrest and apoptosis in EGFRmt TKI-sensitive lung cancer cells (Fig. 8e)[47]. We demonstrate that when *CDK4* or *CDK6* genes are upregulated, EGFRmt lung cancer cells no longer arrest in G1 upon EGFR TKI treatment and instead continue cell cycle progression and become relatively resistant to EGFR targeted therapy (Fig. 8f). These data demonstrate that *CDK4* or *CDK6* overexpression and/or amplification cooperate with the EGFR pathway as convergent regulators of G1/S progression but play a more significant role in EGFR tumor biology than simply allowing the cells to overcome the G1 arrest induced by EGFR inhibition. Early entry into S phase of the cell cycle promoted by *CDK4/6* overexpression and/or amplification can promote replication stress within tumor cells, as evidenced by increased p-Rb1, EdU incorporation, Ki67 and TPX2 expression. Upregulation of TPX2, which is a transcriptional target of E2F transcription factors[32,33], is associated with AURORA Kinase A activation and EGFR

17

TKI resistance[48], suggesting that this is one potential mechanism by which CDK4/6 upregulation may promote EGFR inhibitor resistance (Fig. 8f). The aberrant G1/S checkpoint and consequent replication stress induced by CDK4 or CDK6 overexpression leads to an accumulation of DNA damage, as evidenced by upregulation of pATM, pRPA and gamma-H2AX expression, which in turn leads to increased DNA replication stress response and a DDR (Fig. 8f). Activation of the DDR-related ATM pathway has been shown to promote tumor cell survival during EGFR inhibitor treatment, providing another potential mechanism through which CDK4/6 upregulation may induce EGFR inhibitor resistance[39]. These DNA repair mechanisms may allow CDK4 or CDK6 overexpressing tumor cells to resolve DNA damage to a sufficient level to allow mitosis to proceed, as partially evidenced by a higher mitotic index in CDK4 and CDK6 upregulated tumor xenografts (Fig. 2c-e). In this regard, inhibition of the DDR ATM pathway induced more durable responses in NSCLC *in vivo* models treated with EGFR targeted therapy, indicating a dependence and vulnerability in EGFRmt tumors that may be linked to the CDK4/6-mediated effects we report[39].

The accumulation of karyotypic aberrations associated with CDK4/6 upregulation occurs concurrent with the increased whole genome doubling (WGD) and upregulation of the G2/M checkpoint (Fig. 1h and Fig. 3a). Therefore, these tumor cells undergoing mitosis and division have a high fraction of genome alterations. The increased genomic instability in the context of concurrent *CDK4/6* amplification increases a pool of secondary oncogenic CNAs and mutations which each and in concert promote EGFR TKI resistance; examples include *EGFR*, *CDK6*, *MET* and *BRAF* gene copy number gains and enrichment in TGF-β, NRF-2, RTK/RAS and WNT pathway mutations (Fig. 8f and Supplementary Fig. 12c-e)[15]. Upfront combination therapy with EGFR and CDK4/6 inhibitors could suppress CDK4/6-driven GIN and ongoing evolution in

18

tumors harboring these concurrent genetic alterations. We find evidence for this in the decreased Ki67, RS, DNA damage, and FGA observed upon combinatorial treatment with osimertinib and palbociclib in CDK4/6 overexpressing EGFRmt CDXs and *CDK6* amplified EGFRmt PDXs (Fig. 8g). Combinatorial treatment reduced the proportion of CDK4- and phospho-Rb expressing cells as well as GIN, compared to osimertinib monotherapy, in CDK4 overexpressing EGFRmt tumors (Fig. 6c-j), inducing apoptosis (Fig. 8b) and necrosis in the CDK4/6 overexpressing tumors (Fig. 6k,l and Supplementary Fig. 14e). Based on our data, one possible explanation for these findings is that the combination therapy results in negative selection of clonal and sub-clonal cell populations that harbor CDK4/6 upregulation and the downstream GIN and resistance-associated genomic alterations that accompany it (Fig. 6g-j and Fig. 7e-g).

Of note, we identified *CCNE1* amp, but not *CDK2,* in 5% of FM cases. *CCNE1* amp was mutually exclusive with *CDK4* and *CDK6* amp respectively in 97% and 95% of FM patients. Furthermore, *CCNE1* amp was not associated with significant changes in tumor FGA compared to *CCNE1* wild type cases, suggesting a different mechanism than *CDK4/6* amplification to induce EGFR TKI resistance, which is an area for future study.

Our study has limitations. First, we analyzed tumor DNA through WES or targeted exome sequencing, potentially masking the detection of sub-clonal populations with low abundance and limiting the analysis to the coding DNA regions. Copy number fluctuation of trans- and cis-intronic regulatory elements might also contribute to the evolution of TKI resistance in *CDK4/6* amp, EGFRmt NSCLC and will be a subject of future analyses[49]. We also limited our investigation to canonical roles of CDK4/6 as cell cycle regulators, whereas their functions in regulating gene expression, cell metabolism and immune editing[50] will be further evaluated in expanded clinical cohorts, including other cancer types.

In summary, our study highlights the impact of *CDK4/6* amplification on replication stress and GIN in EGFRmt NSCLC, which persists upon EGFR TKI treatment and contributes to therapy resistance. Combination therapies that block both EGFR and CDK4/6 activity may prevent RS and GIN induced activation of TPX2 and ATM, known contributors to EGFR TKI resistance[39,48]. Reduction in GIN may in turn decrease the pool of GIN-associated secondary alterations that can contribute to EGFR TKI resistance (e.g., *MET* and *BRAF* gene amplifications), promoting more enhanced anti-tumor responses (Fig. 8g). More broadly, our study highlights the complex genetic interactions within cancers that can exert multifactorial downstream biological consequences and contribute to the limited long-term efficacy of therapies that target individual oncogenic-driver alterations such as oncogenic EGFR.

Online Methods

Cell Lines, Primary Organoids and Reagents

All cell lines were obtained and cultured as recommended by the American Type Culture Collection (ATCC). Before testing, cell lines were authenticated through STR profiling and confirmed negative for mycoplasma contamination. EGFR mutant (EGFRmt) NSCLC cell lines used in the present study were H1975 (EGFR L858R, T790M), HCC827 (EGFR Del19), PC9 (EGFR Del19). EGFRmt cells were cultured in RPMI 1640 medium (HyClone, GE Healthcare), containing 10% FBS (SAFC, Sigma-Aldrich) and 1X penicillin and streptomycin (HyClone, GE Healthcare). DMEM (HyClone, GE Healthcare) supplemented with 10% FBS, 0.1X penicillin and streptomycin was used for HEK293-FT cells and SAGM medium (Lonza) for AALE cells. All cell lines were cultured in a humidified incubator with 5% CO_2 at 37 °C. Primary, patient-derived

20

organoid TH-107 cells were established from biopsy specimen and cultured in matrigel as described previously[51,52]. Drugs used in these studies were: Osimertinib, Abemaciclib (Selleckchem); Palbociclib (LC Laboratories). The antibodies used for immunoblotting, immunohistochemistry and immunofluorescence were: CDK4 (Cell Signaling Tech., 12790) CDK6 (Cell Signaling Tech., 3136), pEGFR-Tyr1086 (ThermoFisher, 369700), p-EGFR-Tyr1068 (Cell Signaling Tech., 3777), EGFR L858R (Cell Signaling Tech., 3197), p-AURKA (Cell Signaling Tech., 3079), p-Akt (Cell Signaling Tech., 4060), p-ERK (Cell Signaling Tech., 4370), Actin (Sigma, A2228), Rb (Cell Signaling Tech., 9309), p-Rb-Ser780 (Cell Signaling Tech., 9307), p-Rb-Ser807/811 (Cell Signaling Tech., 8516), CCNE1 (Cell Signaling Tech., 20808), TPX2 (Cell Signaling Tech., 12245), p-RPA (Bethyl Laboratories, A300 245A M), p-ATM (Cell Signaling Tech., 13050 and Sigma, HPA005487), RPA (Bethyl Laboratories, A300 244A), gamma-H2AX (EMD Millipore, 05-636), gamma-Tubulin (Sigma, T5326), ki67 (Leica, NCL-L-Ki67-MM1). Small interfering RNAs for E2F1 and scramble control were purchased from Dharmacon and transient knock-down was induced following the manufacturer's instructions.

Lentiviral Infection, Soft Agar, and Crystal Violet Assays

Mammalian expression vectors EGFP, CDK4, CDK6 were purchased from Origene. Transfection of HEK293-FT cells with the overexpressing vectors was performed using Mirus reagent, per manufacturer's instructions. Viral particles were collected after 72 hrs transfection and used to infect EGFRmt NSCLC cells in medium containing polybrene (8 µg/ml; Sigma-Aldrich). After 72 hrs, cells were either sorted for EGFP or selected with puromycin (1 µg/mL; Gibco). Selected cells were used in the in vitro and in vivo tests. Successful overexpression of CDK4 and CDK6 were confirmed by qPCR and/or immunoblotting.

In vitro, soft agar colony formation assay was performed as previously described[53]. Colonies growth was assessed in a timeframe up to 4 weeks. At the time of collection, 6-well soft agar plates were incubated with a solution of 0.005% crystal violet in water for three hours. Plates were then imaged using ImageQuant (GE Healthcare) and colonies were counted using ImageJ program (NIH).

Preclinical Studies

H1975, PC9 xenografts and TH-116 PDXs were established in compliance with the UCSF IACUC IRB-approved protocols. Each H1975 and PC9 flank xenograft was obtained after sub-cutaneous injection of 1 million cells in the flank of each 4-week-old female SCID or athymic mouse. NSG mice were used for propagation and establishment of TH-116 PDXs. Drug treatments were performed as follows: osimertinib (daily oral gavage, 2.5 mg/Kg, 5 mg/Kg or 10 mg/Kg); palbociclib (daily oral gavage, 100 mg/Kg or 150 mg/Kg). Mice euthanasia was done when xenografts reached 20 mm diameter. We used similar drug regimens for combination studies. Mice were randomly divided and kept unlabeled until the treatments started. The tumors were measured with a digitized caliper by multiple researchers.

For assessing the degree of newly synthetized DNA, IP injections of 100 µL EdU (200 µg) solution in PBS were carried 48 hrs before xenografts resection (Click-iT EdU kit, Invitrogen)[54]. OCT blocks of tissues were collected from each tumor and used for deriving cryosections that were stained either following the manufacture's protocol for single EdU stain (Click-iT EdU kit, Invitrogen) or double immunofluorescence stain with gamma-H2AX[55].

RNA sequencing and GSEA

Total RNAs were extracted from CDK4/6 overexpressing tissues and empty vector controls (Qiagen) and sent to Novogene for RNA sequencing (NovaSeq 6000, PE150).

For the Gene Set Enrichment Analysis (GSEA), a gene expression matrix for CDK4, CDK6 overexpressing tissues, and controls (cells expressing empty vector, E.V.), in triplicates, was imported into GSEA algorithm (v4.03, Broad Institute). MSigDB was used for gene set enrichment comparisons between CDK4/6 overexpressing and E.V. CDXs groups. The enrichment score (ES), normalized ES and False discovery rate (FDR) were provided from the algorithm. An FDR < 25% was used for exploratory enrichment analysis.

Immunoblotting, Immunohistochemistry, Immunofluorescence and FUCCI assay

Protein lysates were extracted in RIPA buffer, adding protease inhibitors (Roche) and phosphatase inhibitors (Roche). For the immunoblotting, 15 μg of proteins were loaded into precast 4–15% acrylamide gels (Bio-Rad), then transferred on nitrocellulose membranes with Trans-blot Turbo Transfer system (Bio-Rad). Blots were blocked for 1 hr at room temperature in Tris-buffered saline, 0.1% Tween20 (vol/vol) and 5% (vol/vol) BSA (Fisher Scientific). Incubation with the primary antibodies was performed overnight at 4 °C, after which the membranes were washed twice with Tris-buffered saline, Tween20 (0.1% vol/vol). Incubation with secondary HRP-conjugated antibodies (Cell Signaling Technology, anti-rabbit IgG, no. 7074, anti-mouse IgG, no. 7076) was run for 1 hr, at room temperature. Membranes were then incubated with ECL reagent (GE Healthcare) and the signal detected by chemiluminescence. The development and scanning of the blots were run with ImageQuant LAS4000 (GE Healthcare Life Sciences). ImageJ (NIH) allowed western blot quantification.

Formalin-Fixed, Paraffin Embedded tissue blocks and sections were provided by the UCSF histology core. Immunohistochemistry (IHC) was performed as previously described [3]. The stained slides were scanned with Aperio ScanScope CS Slide Scanner (Aperio Technologies) using a 20x objective. ScanScope algorithm was applied for the IHC quantification considering 3-5 fields per section and calculating mean and S.E.M. CDK4, CDK6, pRb, γ-H2AX, pRPA stains were quantified on same areas of adjacent xenograft, viable tissue sections. Immunofluorescence with gamma-Tubulin antibody was performed using cryosections from OCT blocks collected from H1975 tissue xenografts as previously described[56].

For the tissue necrotic area analysis, FFPE sections were stained with hematoxylin-eosin and necrosis was quantified as percentage of affected areas following pathological guidelines[57].

Premo FUCCI dual sensor (Invitrogen) assay was used for assessing the cell cycle stage in E.V. and CDK6 overexpressing HCC827 single cells[28]. Briefly, cells were transfected with the sensor plasmids for 24 hrs, following the manufacturer's instructions, then cells were seeded in soft agar. Fluorescent cells were imaged using a Zeiss Axioplan II microscope. Cells at different cell cycle stages were quantified with ImageJ (NIH) and expressed as a percentage of the whole population.

Karyotyping Analyses: Metaphase Spreads, pan-centromeres FISH, PI-Flow Cytometry

Metaphase spreads from AALE and H1975 cells were prepared as previously described[58]. Spreads were imaged with a Nikon Ti inverted microscope using a 100X objective and chromosomes were counted using ImageJ software (NIH). Pan-centromere probe (PNA Bio) FISH was performed on fixed cells and FFPE[59] according to the manufacturer's instructions. Propidium iodide DNA staining and flow cytometry analysis were carried using xenograft derived single cell, prepared as previously described[60], fixed in ethanol 70% then stained with a propidium iodide solution

24

(Sigma). Single cell PI quantification was run using a FACSCalibur flow cytometer and data were analyzed with FlowJo software.

Fraction of Genome Alteration Analysis (FGA), SNVs and copy number calling from whole exome sequencing data from in vivo tumor tissues

DNA was extracted from xenograft tissues using tissue-DNA extraction-specific kit (Qiagen) and sent to Novogene (Sacramento, USA) for whole exome sequencing (WES; NovaSeq 6000, PE150, 200X). Pair-end fastq files were mapped to the hg19 genome. Mutation (SNVs) calling was done using the SeqMule pipeline. The vcf files were annotated using ANNOVAR software at a high-performance computing cluster (UCSF Helen Diller Comprehensive Cancer Center). Further analysis of annotated variants was conducted under the RStudio/R environment. Cell-derived and patient-derived xenograft WES bam files were used to infer copy number alterations between treatment group and control group utilizing function "copynumber" in VarScan algorithm. The altered genomic segments were annotated at gene levels. Each gene length was retrieved from hsapiens.UCSC.hg19.knownGene database. The sum of altered CNA genes over size of captured WES was defined as Fraction of Genome Alteration (FGA). We normalized the CDK4/6 overexpressing and CDK6 amp xenografts FGA with the FGA from empty vector, CDK4/6 wild type or vehicle treated control xenografts expressing it as a fold-change[23]. To infer absolute integer gene copy number, mapped BAM files were used as input along with hg19_SureSelect_Human_All_Exon_V5.bed and human_g1k_v37.fasta files, for CNVkit (default parameters, python library, https://cnvkit.readthedocs.io/en/stable/), and log2 ratio of estimated segmentation between two conditions was computed.

Foundation Medicine, MSK Impact and cBioPortal dataset analyses

EGFRmt advanced stage NSCLC cases analyzed from Foundation Medicine (FM) were 660 and targeted exome sequencing data for a panel of 401 cancer-related genes were used to detect somatic mutations and copy number alteration. The annotated data matrix was provided from FM. FGA analysis was computed from FM dataset using a panel of 306 cancer-related gene with CNV (gains and deletions) following previously published methods[23]. Briefly, patients were stratified based on the presence of selected cell cycle gene copy number alterations[22]. For each patient, genes with copy number alterations annotated from FM were filtered in and the size of each gene retrieved. The sum of altered gene sizes over the captured genome was computed as FGA. Boxplots were created with interquartile range (lower quartile 25%, median and upper quartile 75%). Each dot represents the FGA value in each patient's tumor. Statistical significance was assessed using Wilcoxon test. For the Tumor Mutation Burden (TMB) analysis, the total nonsynonymous mutations over the captured genome size were computed as tumor mutation burden (TMB, number of gene mutations/Mega-base).

FGA analysis was computed from MSK IMPACT dataset using 1668 NSCLC cases stratified in EGFRmt NSCLC cases carrying concurrent Cell Cycle alterations (69) or negative for such alterations (339) and from GENIE MSK IMPACT dataset using 1657 NSCLC LUAD EGFRmt patient's tumors stratified in *CDK4/6* amp positive (128) or negative (1469).

For the correlation analysis between FGA and *CDK4/6* amplifications, patients harboring *CDK4/CDK6* amplifications with copy number greater that 4 were selected, the value of log10(CNV *CDK4/6* amp) versus FGA value were plotted with linear regression model for best fit line, and F-statistics was used to calculate p-value.

Oncoprint analysis was used to show the most frequent concurrent gene alterations in Cell Cycle (CC) alteration positive (n=357) or CC-alteration negative (n=303) Foundation Medicine dataset cohorts. Each column represents a patient, each row represents one gene. Gene alteration frequencies greater than 6% were shown in the oncoprints.

Analysis of LUAD cases through cBioPortal was done selecting cases positive for *CDK4/6* CNAs, with concurrent *EGFR* mutations or wild type *EGFR*. Cases with concurrent *EGFR* and *CDK4/6* alterations were further analyzed for frequencies of *Rb1* alterations.

Whole Genome Doubling (WGD) analysis

Whole Genome Doubling (WGD) analysis from TCGA lung adenocarcinoma (LUAD) cohort dataset was downloaded from:

https://github.com/judithabk6/ITH_TCGA/blob/master/external_data/TCGA_mastercalls.abs_tables_JSedit.fixed.txt

Correlation analysis was run annotating WGD events along with the status of *CDK4/6* amp. Fisher exact test was used for the statistical significance.

Statistical analyses

We used One-way ANOVA with Tukey's multiple comparisons and Student's T-test to assess statistical significance in preclinical functional studies (GraphPad Prism); variations across samples were expressed as S.E.M. For the Fraction of Genome Alterations (FGA) and Tumor Mutational Burden (TMB) analyses, statistical significance was assessed by Wilcoxon non-parametric two group comparison test and two-side student t-test.

References

1. Katti, A., Diaz, B.J., Caragine, C.M., Sanjana, N.E. & Dow, L.E. CRISPR in cancer biology and therapy. *Nat Rev Cancer* **22**, 259-279 (2022).
2. van de Haar, J. *et al.* Identifying Epistasis in Cancer Genomes: A Delicate Affair. *Cell* **177**, 1375-1383 (2019).
3. Blakely, C.M. *et al.* Evolution and clinical impact of co-occurring genetic alterations in advanced-stage EGFR-mutant lung cancers. *Nat Genet* **49**, 1693-1704 (2017).
4. Turajlic, S., McGranahan, N. & Swanton, C. Inferring mutational timing and reconstructing tumour evolutionary histories. *Biochim Biophys Acta* **1855**, 264-75 (2015).
5. Siegel, R.L., Miller, K.D., Fuchs, H.E. & Jemal, A. Cancer Statistics, 2021. *Ca-a Cancer Journal for Clinicians* **71**, 7-33 (2021).
6. Molina, J.R., Yang, P.G., Cassivi, S.D., Schild, S.E. & Adjei, A.A. Non-small cell lung cancer: Epidemiology, risk factors, treatment, and survivorship. *Mayo Clinic Proceedings* **83**, 584-594 (2008).
7. Ganti, A.K., Klein, A.B., Cotarla, I., Seal, B. & Chou, E. Update of Incidence, Prevalence, Survival, and Initial Treatment in Patients With Non-Small Cell Lung Cancer in the US. *JAMA Oncol* **7**, 1824-1832 (2021).
8. Tan, A.C. & Tan, D.S.W. Targeted Therapies for Lung Cancer Patients With Oncogenic Driver Molecular Alterations. *Journal of Clinical Oncology* **40**, 611-625 (2022).
9. Lynch, T.J. *et al.* Activating mutations in the epidermal growth factor receptor underlying responsiveness of non-small-cell lung cancer to gefitinib. *New England Journal of Medicine* **350**, 2129-2139 (2004).
10. Paez, J.G. *et al.* EGFR mutations in lung cancer: Correlation with clinical response to gefitinib therapy. *Science* **304**, 1497-1500 (2004).
11. Pao, W. *et al.* Acquired resistance of lung adenocarcinomas to gefitinib or erlotinib is associated with a second mutation in the EGFR kinase domain. *Plos Medicine* **2**, 225-235 (2005).

12. Ramalingam, S.S. *et al.* Overall Survival with Osimertinib in Untreated, EGFR-Mutated Advanced NSCLC. *New England Journal of Medicine* **382**, 41-50 (2020).

13. Soria, J.C. *et al.* Osimertinib in Untreated EGFR-Mutated Advanced Non-Small-Cell Lung Cancer. *New England Journal of Medicine* **378**, 113-125 (2018).

14. Thress, K.S. *et al.* Acquired EGFR C797S mutation mediates resistance to AZD9291 in non-small cell lung cancer harboring EGFR T790M. *Nature Medicine* **21**, 560-562 (2015).

15. Gini, B., Thomas, N. & Blakely, C.M. Impact of concurrent genomic alterations in epidermal growth factor receptor (EGFR)-mutated lung cancer. *Journal of Thoracic Disease* **12**, 2883-2895 (2020).

16. Liu, M.H. *et al.* PD 0332991, a selective cyclin D kinase 4/6 inhibitor, sensitizes lung cancer cells to treatment with epidermal growth factor receptor tyrosine kinase inhibitors. *Oncotarget* **7**, 84951-84964 (2016).

17. Sitthideatphaiboon, P. *et al.* Co-occurrence CDK4/6 amplification serves as biomarkers of de novo EGFR TKI resistance in sensitizing EGFR mutation non-small cell lung cancer. *Sci Rep* **12**, 2167 (2022).

18. Ekholm, S.V. & Reed, S.I. Regulation of G(1) cyclin dependent kinases in the mammalian cell cycle. *Current Opinion in Cell Biology* **12**, 676-684 (2000).

19. Zhang, C.-Z. & Pellman, D. Cancer Genomic Rearrangements and Copy Number Alterations from Errors in Cell Division. *Annual Review of Cancer Biology* **6**, 245-268 (2022).

20. Abbas, T., Keaton, M.A. & Dutta, A. Genomic instability in cancer. *Cold Spring Harb Perspect Biol* **5**, a012914 (2013).

21. Panagopoulos, A. & Altmeyer, M. The Hammer and the Dance of Cell Cycle Control. *Trends Biochem Sci* **46**, 301-314 (2021).

22. Sanchez-Vega, F. *et al.* Oncogenic Signaling Pathways in The Cancer Genome Atlas. *Cell* **173**, 321-+ (2018).

23. Zhou, J. *et al.* Analysis of Tumor Genomic Pathway Alterations Using Broad-Panel Next-Generation Sequencing in Surgically Resected Lung Adenocarcinoma. *Clin Cancer Res* (2019).

24. Hanahan, D. & Weinberg, R.A. Hallmarks of cancer: the next generation. *Cell* **144**, 646-74 (2011).

25. Lau, T.Y. & Poon, R.Y.C. Whole-Genome Duplication and Genome Instability in Cancer Cells: Double the Trouble. *Int J Mol Sci* **24**(2023).

26. Niederst, M.J. *et al.* RB loss in resistant EGFR mutant lung adenocarcinomas that transform to small-cell lung cancer. *Nat Commun* **6**, 6377 (2015).

27. Lee, J.K. *et al.* Clonal History and Genetic Predictors of Transformation Into Small-Cell Carcinomas From Lung Adenocarcinomas. *J Clin Oncol* **35**, 3065-3074 (2017).

28. Fischer, L. & Thievessen, I. FUCCI Reporter Gene-Based Cell Cycle Analysis. *Methods Mol Biol* **2644**, 371-385 (2023).

29. Dasika, G.K. *et al.* DNA damage-induced cell cycle checkpoints and DNA strand break repair in development and tumorigenesis. *Oncogene* **18**, 7883-7899 (1999).

30. Ren, L.Q. *et al.* Potential biomarkers of DNA replication stress in cancer. *Oncotarget* **8**, 36996-37008 (2017).

31.   Byrum, A.K. *et al.* Mitotic regulators TPX2 and Aurora A protect DNA forks during replication stress by counteracting 53BP1 function. *Journal of Cell Biology* **218**, 422-432 (2019).

32.   Rouillard, A.D. *et al.* The harmonizome: a collection of processed datasets gathered to serve and mine knowledge about genes and proteins. *Database (Oxford)* **2016**(2016).

33.   Lachmann, A. *et al.* ChEA: transcription factor regulation inferred from integrating genome-wide ChIP-X experiments. *Bioinformatics* **26**, 2438-44 (2010).

34.   Haderk, F. *et al.* A focal adhesion kinase-YAP signaling axis drives drug tolerant persister cells and residual disease in lung cancer. *bioRxiv*, 2021.10.23.465573 (2021).

35.   Eisenhauer, E.A. *et al.* New response evaluation criteria in solid tumours: revised RECIST guideline (version 1.1). *Eur J Cancer* **45**, 228-47 (2009).

36.   Oxnard, G.R. *et al.* TATTON: a multi-arm, phase Ib trial of osimertinib combined with selumetinib, savolitinib, or durvalumab in EGFR-mutant lung cancer. *Ann Oncol* **31**, 507-516 (2020).

37.   Leonetti, A. *et al.* Resistance mechanisms to osimertinib in EGFR-mutated non-small cell lung cancer. *Br J Cancer* (2019).

38.   Khalil, A.I.S., Khyriem, C., Chattopadhyay, A. & Sanyal, A. Hierarchical discovery of large-scale and focal copy number alterations in low-coverage cancer genomes. *BMC Bioinformatics* **21**, 147 (2020).

39.   Ali, M. *et al.* Small-molecule targeted therapies induce dependence on DNA double-strand break repair in residual tumor cells. *Sci Transl Med* **14**, eabc7480 (2022).

40.   Caswell, D.R. *et al.* The role of APOBEC3B in lung tumor evolution and targeted cancer therapy resistance. *Nat Genet* **56**, 60-73 (2024).

41.   Yu, H.A. *et al.* Concurrent Alterations in EGFR-Mutant Lung Cancers Associated with Resistance to EGFR Kinase Inhibitors and Characterization of MTOR as a Mediator of Resistance. *Clin Cancer Res* **24**, 3108-3118 (2018).

42.   Ma, C.S. *et al.* NRF2-GPX4/SOD2 axis imparts resistance to EGFR-tyrosine kinase inhibitors in non-small-cell lung cancer cells. *Acta Pharmacol Sin* **42**, 613-623 (2021).

43.   Zhang, Y. *et al.* The canonical TGF-beta/Smad signalling pathway is involved in PD-L1-induced primary resistance to EGFR-TKIs in EGFR-mutant non-small-cell lung cancer. *Respir Res* **20**, 164 (2019).

44.   Jamal-Hanjani, M. *et al.* Tracking the Evolution of Non-Small-Cell Lung Cancer. *N Engl J Med* **376**, 2109-2121 (2017).

45.   Frankell, A.M. *et al.* The evolution of lung cancer and impact of subclonal selection in TRACERx. *Nature* **616**, 525-533 (2023).

46.   Wee, P. & Wang, Z. Epidermal Growth Factor Receptor Cell Proliferation Signaling Pathways. *Cancers (Basel)* **9**(2017).

47.   Cross, D.A. *et al.* AZD9291, an irreversible EGFR TKI, overcomes T790M-mediated resistance to EGFR inhibitors in lung cancer. *Cancer Discov* **4**, 1046-61 (2014).

48.   Shah, K.N. *et al.* Aurora kinase A drives the evolution of resistance to third-generation EGFR inhibitors in lung cancer. *Nat Med* **25**, 111-118 (2019).

49.   Agustinus, A.S. *et al.* Epigenetic dysregulation from chromosomal transit in micronuclei. *Nature* (2023).

50. Fassl, A., Geng, Y. & Sicinski, P. CDK4 and CDK6 kinases: From basic science to cancer therapy. *Science* **375**, eabc1495 (2022).

51. Seino, T. *et al.* Human Pancreatic Tumor Organoids Reveal Loss of Stem Cell Niche Factor Dependence during Disease Progression. *Cell Stem Cell* **22**, 454-+ (2018).

52. Barbosa Rabago, D., Blakely, C.M., Haderk, F. & Bivona, T.G. Profiling Sensitivity to Targeted Therapies in EGFR-Mutant NSCLC Patient-Derived Organoids. *J Vis Exp* (2021).

53. Horibata, S., Vo, T.V., Subramanian, V., Thompson, P.R. & Coonrod, S.A. Utilization of the Soft Agar Colony Formation Assay to Identify Inhibitors of Tumorigenicity in Breast Cancer Cells. *Jove-Journal of Visualized Experiments* (2015).

54. Salic, A. & Mitchison, T.J. A chemical method for fast and sensitive detection of DNA synthesis in vivo. *Proceedings of the National Academy of Sciences of the United States of America* **105**, 2415-2420 (2008).

55. Solovjeva, L., Firsanov, D., Pleskach, N. & Svetlova, M. Immunofluorescence Analysis of γ-H2AX Foci in Mammalian Fibroblasts at Different Phases of the Cell Cycle. in *Fast Detection of DNA Damage: Methods and Protocols* (ed. Didenko, V.V.) 187-194 (Springer New York, New York, NY, 2017).

56. Gini, B. *et al.* The mTOR kinase inhibitors, CC214-1 and CC214-2, preferentially block the growth of EGFRvIII-activated glioblastomas. *Clin Cancer Res* **19**, 5722-32 (2013).

57. Kumar, V., Abbas, A.K., Fausto, N. & Aster, J.C. *Robbins and Cotran Pathologic Basis of Disease, Professional Edition E-Book*, (Elsevier Health Sciences, 2014).

58. Nathanson, D.A. *et al.* Targeted therapy resistance mediated by dynamic regulation of extrachromosomal mutant EGFR DNA. *Science* **343**, 72-6 (2014).

59. Chin, S.F. *et al.* A simple and reliable pretreatment protocol facilitates fluorescent in situ hybridisation on tissue microarrays of paraffin wax embedded tumour samples. *Journal of Clinical Pathology-Molecular Pathology* **56**, 275-279 (2003).

60. Wei, W. *et al.* Single-Cell Phosphoproteomics Resolves Adaptive Signaling Dynamics and Informs Targeted Combination Therapy in Glioblastoma. *Cancer Cell* **29**, 563-73 (2016).
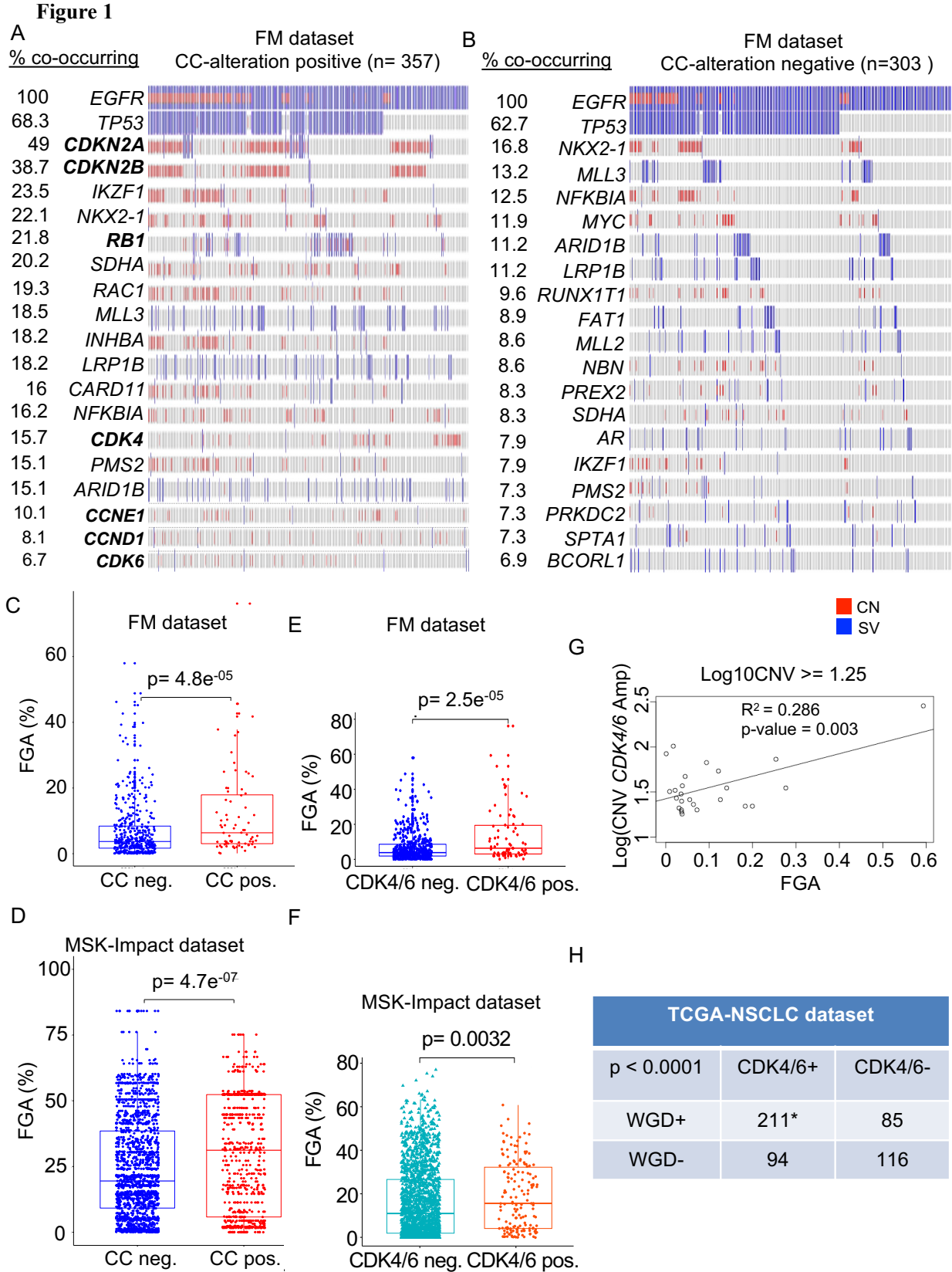
Figure 1

Figure 1 - Concurrent *EGFRmt* and *CDK4/6* CNAs enhance the percentage of genome alterations in NSCLC patient tumors.

(A, B) Oncoprints highlighting recurrent gene alterations detected in advanced EGFRmt NSCLCs harboring cell cycle (CC) gene alterations (CC pos.; A) or negative for such alterations (CC neg.; B) (Foundation Medicine-FM, dataset). (C, D) FGA analysis in EGFRmt NSCLCs using Foundation Medicine targeted exome sequencing (C) or MSK-Impact (D) datasets, stratifying tumors carrying concurrent cell cycle CNAs (CC pos.) versus tumors negative for such alterations (CC neg.). (E, F) FGA analysis in EGFRmt tumors using Foundation Medicine targeted exome sequencing (E) or MSK-Impact (F) datasets, stratifying tumors carrying concurrent *CDK4/6* CNAs (*CDK4/6* pos.) versus patient's tumors negative for such alterations (*CDK4/6* neg.). (G) Positive correlation plot showing degrees of *CDK4/6* amplification (y-axis) and corresponding FGA (p-value calculated with F-statistics). (H) Whole Genome Doubling (WGD) analysis using TCGA data from NSCLC cases carrying *CDK4/6* CNAs or negative for such alterations.

(FGA boxplots represent interquartile range, lower quartile 25%, median and upper quartile 75%; each dot represents the FGA value in each patient's tumor; p-value calculated with Wilcoxon test).

See also Supplementary Figures 1-2.

Figure 2
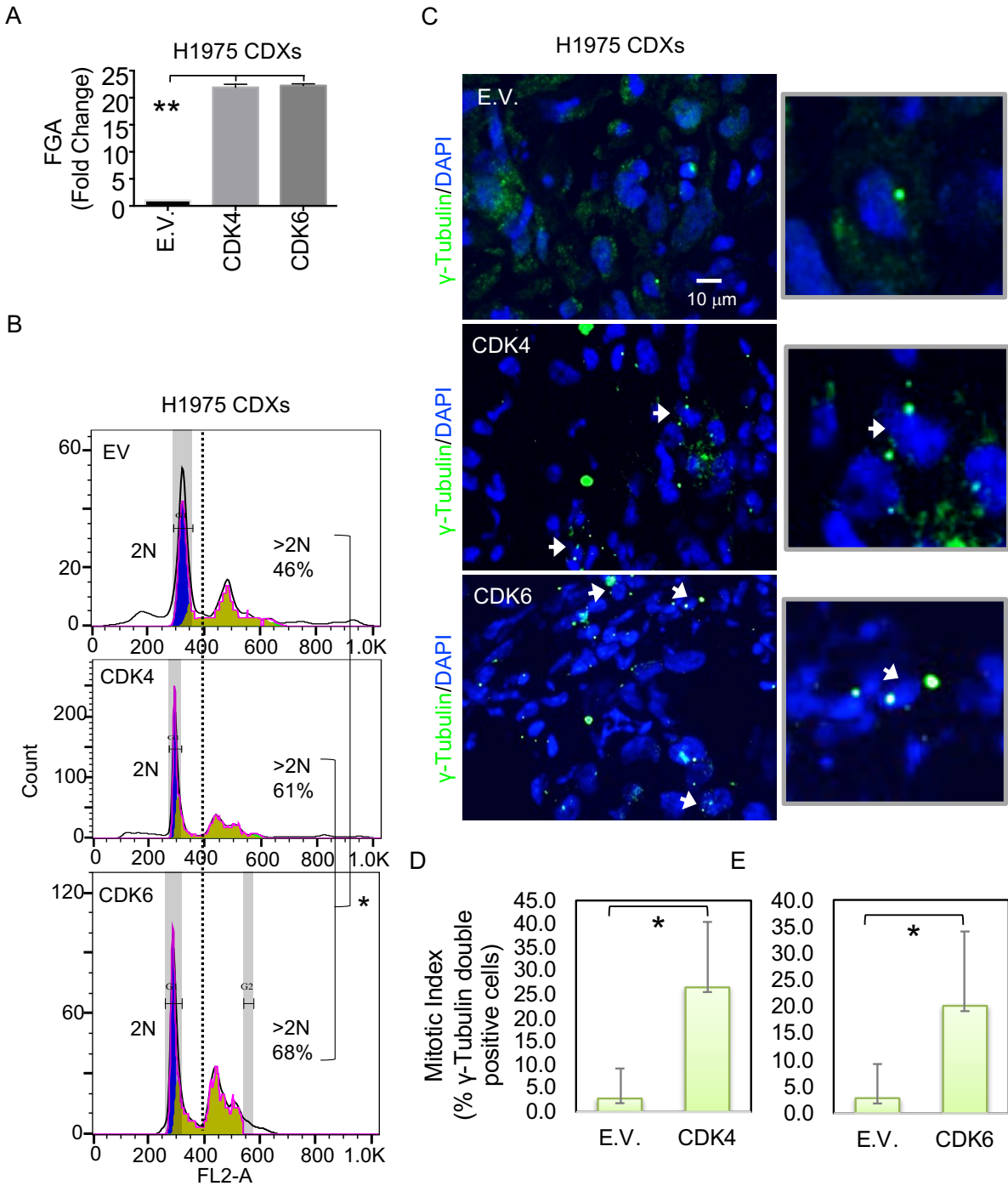
Figure 2 - CDK4/6 upregulation enhances the percentage of genome alterations in NSCLC in vivo models.

(A) Fraction of Genome Alterations (FGA) analysis with whole exome sequencing data from H1975 CDXs genetically engineered to overexpress CDK4 or CDK6 proteins compared to empty vector (E.V.) controls (n = 2 xenografts per group; **$P < 0.0001$; p-value assessed by one-way Anova and Tukey's multiple comparisons test; error bars representing SEM). (B) Single cell karyotype analysis with propidium iodide stain and flow cytometry of fixed cells derived from E.V. and CDK4/6 overexpressing H1975 CDXs (n = 1-2 xenografts per group; *$P = 0.02$, Student's t-test). (C-E) Immunofluorescence assay of γ-tubulin in centrosomes of dividing cells (C); double-centrosome positive, dividing cells quantified in (D-E) and expressed as a percentage of total, single- and double-centrosome positive cells (n = 1 xenograft per group, 4-5 images per tissue; *$P < 0.05$, Student's t-test; error bars representing SD).

(E.V.: empty vector; CDK4: CDK4 overexpressing xenografts; CDK6: CDK6 overexpressing xenografts).

See also Supplementary Figures 3-4.

Figure 3

A

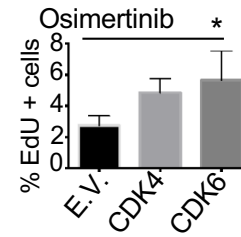| Pathway	NES vs E.V.	
	NES CDK4 V.	CDK6
E2F_TARGETS	3.0660121	3.0148368
G2M_CHECKPOINT	2.6910038	2.3356688
DNA_REPAIR	1.1376647	1.5257235
TNFA_SIGNALING_VIA_NFKB	-3.003705	-2.710381
EPITHELIAL_MESENCHYMAL_TRANSITION	-2.283844	-1.893819
P53_PATHWAY	-1.726412	-1.735833
APOPTOSIS	-1.62453	-1.529128

UP (P-val. < 0.05)
DOWN (P-val. < 0.05)

B
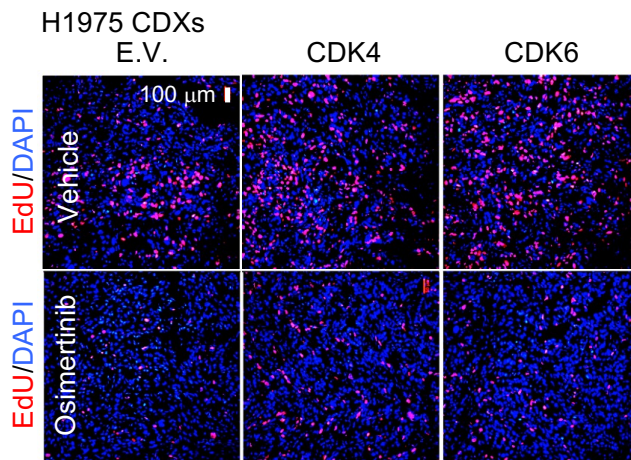
C
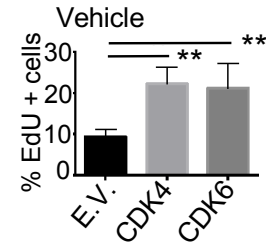
D

E
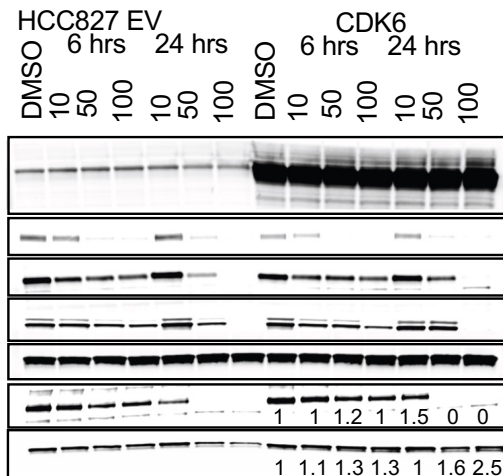
F
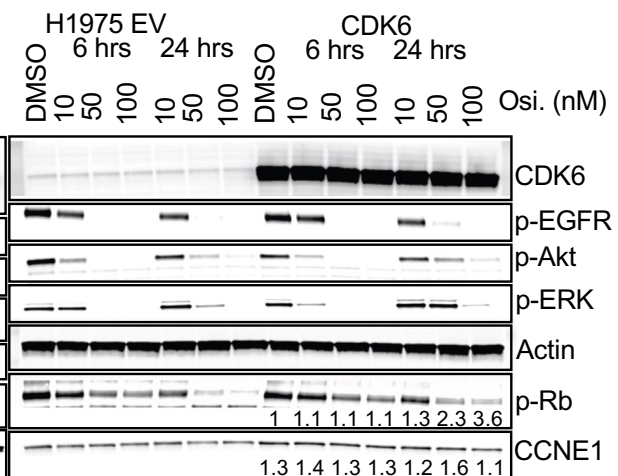
Figure 3 - CDK4/6 upregulation promotes premature DNA synthesis in EGFR mutant in vivo NSCLC models.

(A) GSEA enrichment in H1975 CDK4/6 overexpressing CDXs compared to empty vector (E.V.) controls (n = 3 xenografts per group; p-value calculated as described in methods). (B-D) S-phase and active cell cycle progression analysis in H1975 CDK4/6 overexpressing tumors by quantification of EdU incorporation (B, red dots) in newly synthesized DNA in vehicle (C) and osimertinib-treated (D) tissues (n = 3-4 images/xenograft per group; **P = 0.003, *P = 0.02; p-value assessed by one-way Anova and Tukey's multiple comparisons test). (E-F) Biochemical analysis of G1/S progression biomarkers and EGFR pathway inhibition in dose escalation time course with osimertinib (10-100 nM) using CDK6 overexpressing HCC827 and H1975 cells compared to E.V. controls.
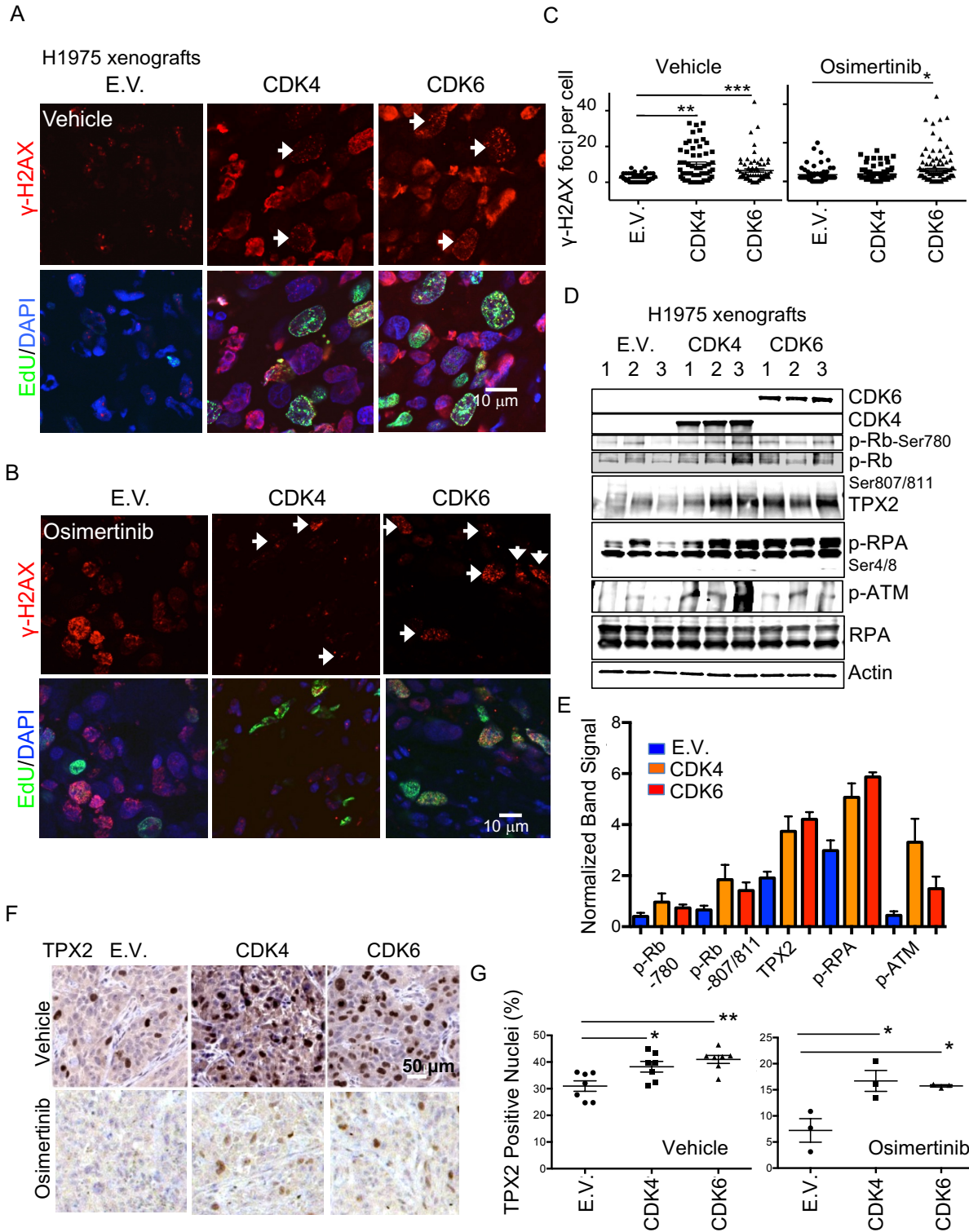
See also Supplementary Figures 5-6.

Figure 4

Figure 4 - CDK4/6 upregulation promotes DNA damage accumulation and RS in EGFR mutant in vivo NSCLC models.

(A-C) Double immunofluorescence stain for γ-H2AX (red) and EdU (green) (A, B) and quantification of γ-H2AX foci number (C) in EdU positive cells for vehicle (A) and osimertinib (B) treated H1975 CDXs (white arrows point to double positive cells; n = 50-100 EdU positive cells per sample, one xenograft per group; ***$P < 0.0001$, **$P < 0.001$, *$P = 0.03$). (D-E) Immunoblotting assay of replication stress biomarkers in CDK4/6 overexpressing H1975 CDXs (D) and relative quantification (E) versus empty vector (E.V.) controls. (F-G) Representative images of TPX2 IHC stain (F) and corresponding quantification (G) using tissues from CDK4/6 overexpressing H1975 CDXs and E.V. controls (n = 3-4 xenografts per group; **$P = 0.003$, *$P < 0.05$).

(p-value calculated with one-way Anova and Tukey's multiple comparisons test).

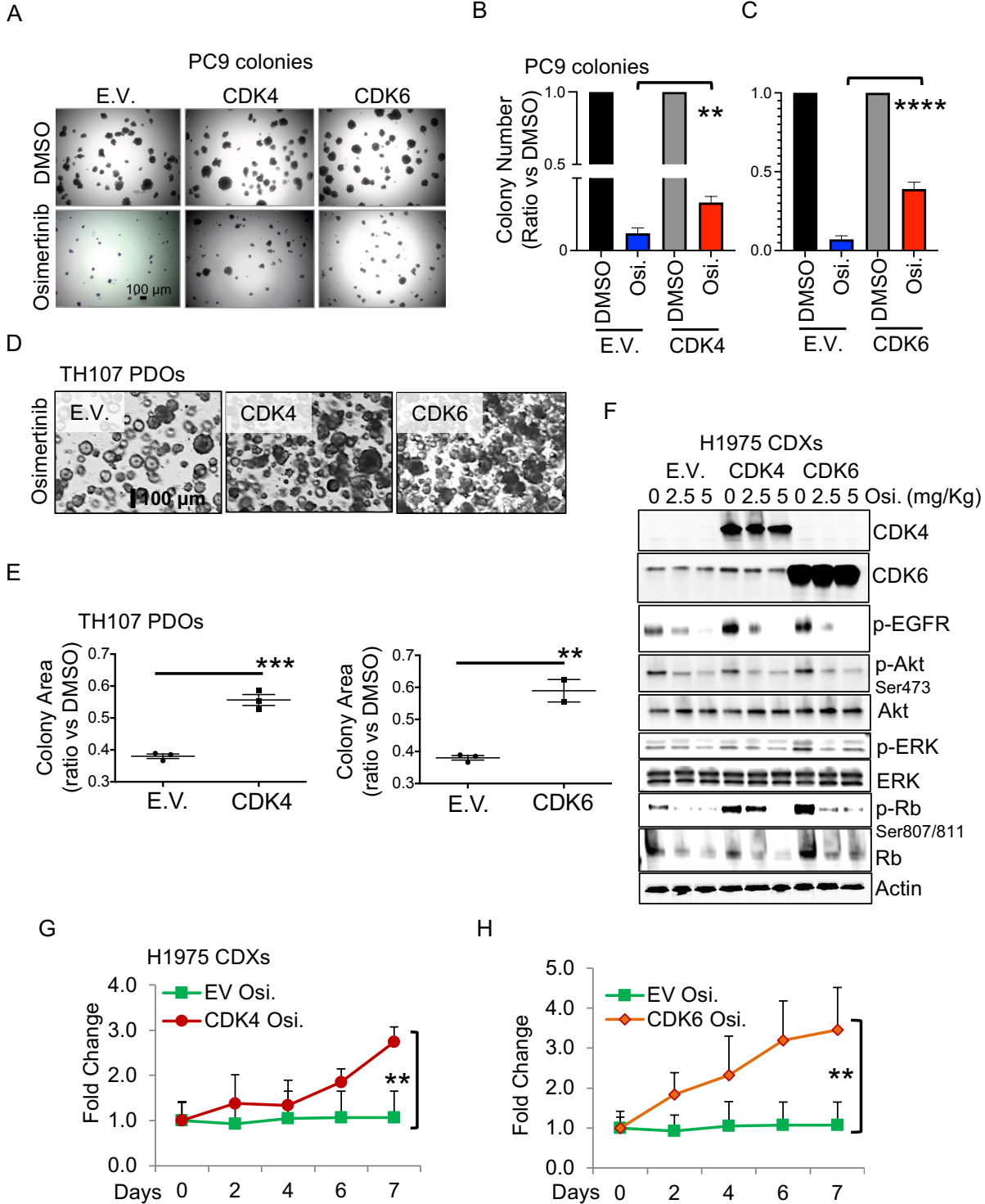See also Supplementary Figure 7.

Figure 5

40

Figure 5 - CDK4/6 upregulation promotes osimertinib resistance in preclinical models of EGFR mutant NSCLC.

(A-C) Soft agar colony formation assay (A) and quantification (B-C) using CDK4/6 overexpressing PC9 (**P = 0.003, ****P < 0.0001) EGFRmt NSCLC cell lines and E.V. control cells (p-value determined using Student's t-test; error bars representing SEM; E.V.: empty vector; CDK4 and CDK6: CDK4 or CDK6 overexpressing cells; Osi.: osimertinib 10 nM - 100 nM). (D-E) Long-term (35 days) osimertinib (500 nM) treatment with genetically modified EGFR Del19 TH107 PDOs to overexpress CDK4 or CDK6 (D) and colony area's quantification (E) (***P = 0.0007, ** P = 0.004, Student's t-test). (F) Biochemical analysis of CDK4/6 overexpressing H1975 CDXs and Empty Vector (E.V.) overexpressing control CDXs, treated with vehicle or osimertinib 2.5-5 mg/Kg, analyzing EGFR and CDK4/6 signaling biomarkers. (G-H) Growth curves of osimertinib (5 mg/Kg) treated CDK4 (G) or CDK6 (H) overexpressing H1975 CDXs compared to empty vector overexpressing controls (**P < 0.01, n = 4 xenografts per group, Student's t-test).

(E.V.: empty vector; CDK6: CDK6 overexpressing PDOs/CDXs; CDK4: CDK4 overexpressing PDOs/CDXs; Osi.: osimertinib; p-value calculated with one-way Anova and Tukey's multiple comparisons).

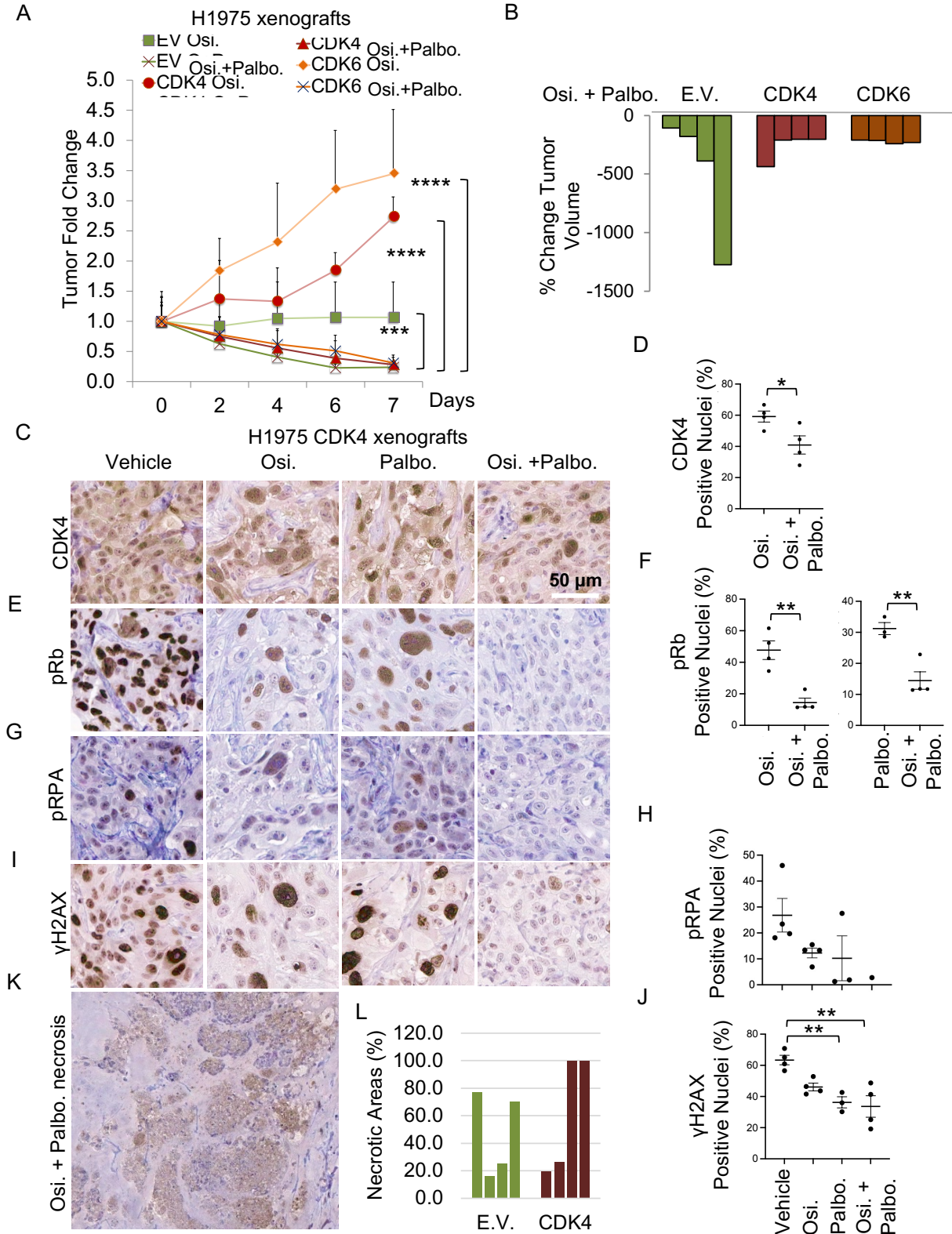See also Supplementary Figures 8-13.

Figure 6

Figure 6 - Combination therapy with EGFR and CDK4/6 inhibitors suppresses tumor growth and decreases GIN and RS in CDK4/6 o/e EGFRmt CDXs.

(A) Growth curves of CDK4/6 overexpressing H1975 and empty vector control CDXs treated with osimertinib (5 mg/Kg) and combinatorial treatments with palbociclib (100 mg/Kg) (n = 4 xenografts per group). Palbociclib treated tumors had similar growth curves than vehicle treated tumors (****P < 0.0001, ***P < 0.001). (B) Percentage of tumor volume change of individual E.V. and CDK4/6 overexpressing H1975 CDXs treated with the combination treatment. (C-J) Representative IHC stain images and quantification of CDK4 (C, D), pRb (E, F), pRPA (G, H), γH2AX (I, J) using tissues from CDK4 overexpressing H1975 CDXs treated with osimertinib (5 mg/Kg) and combinatorial treatments with palbociclib (100 mg/Kg) (n = 3-4 xenografts per group; *P < 0.05, **P < 0.01). (K-L) Representative hematoxylin stain (K) and quantification of necrotic areas in E.V. and CDK4 overexpressing H1975 CDXs treated with combinatorial treatment.

(E.V.: empty vector; CDK4: CDK4 overexpressing CDXs; CDK6: CDK6 overexpressing CDXs; Veh.: vehicle; Palbo.: palbociclib; Osi.: osimertinib; p-value assessed by one-way Anova and Tukey's multiple comparisons test and Student's t-test; error bars representing SEM).

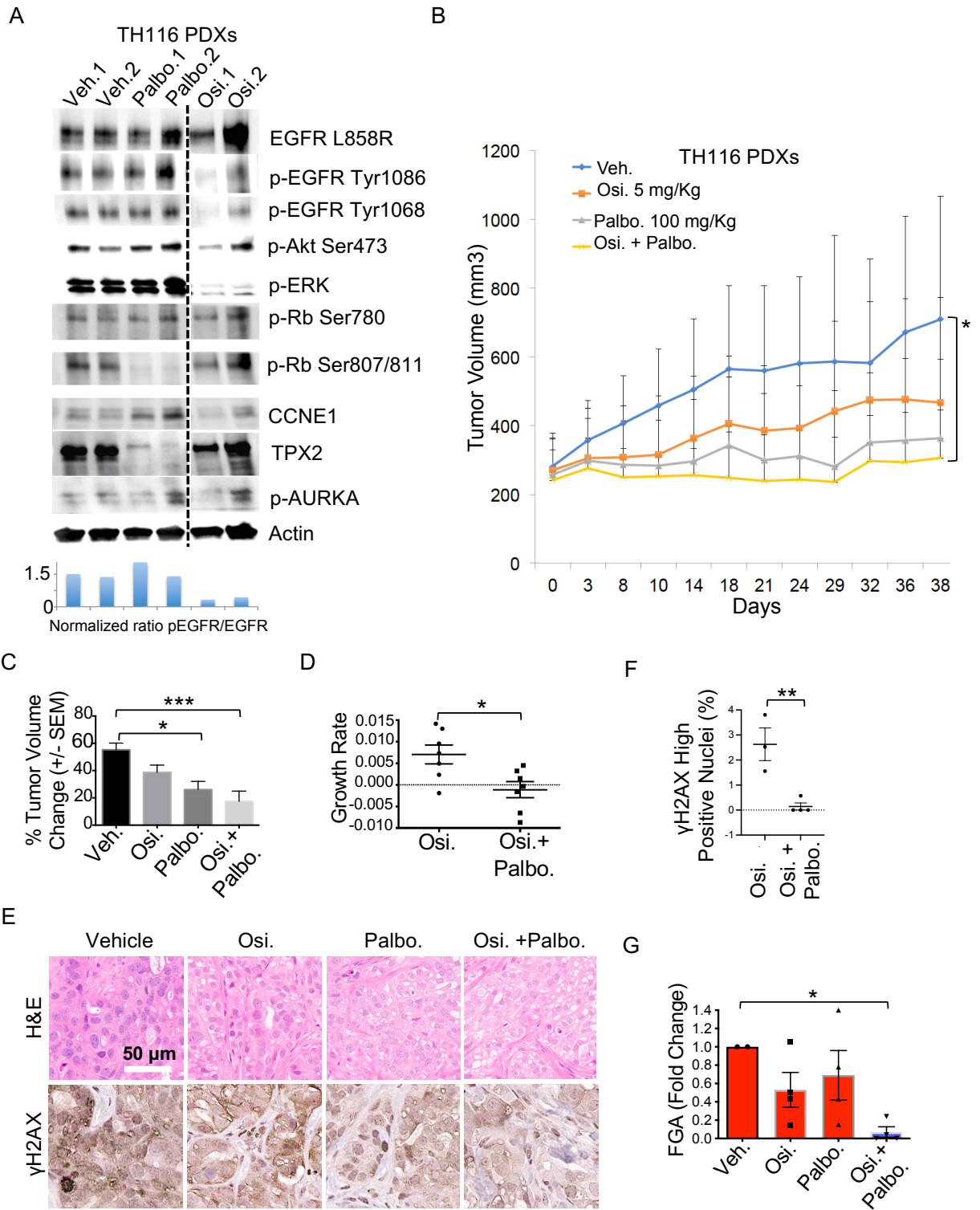See also Supplementary Figures 14.

Figure 7

Figure 7 - Combination therapy with EGFR and CDK4/6 inhibitors suppresses tumor growth and decreases GIN and RS in *CDK6*amp, EGFRmt PDXs.
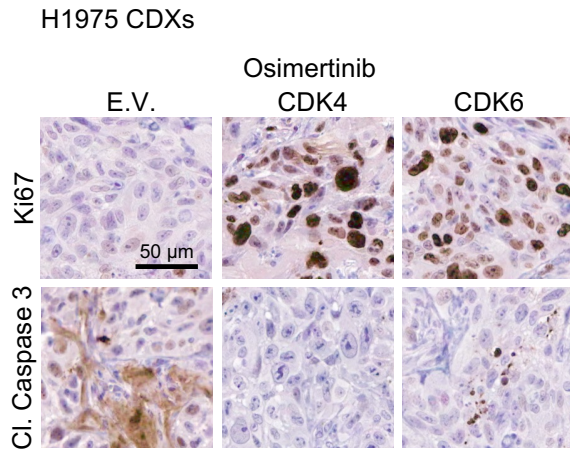
(A) Biochemical assay for EGFR pathway, CDK4/6 signaling and replication stress biomarkers from in vivo experiment with TH116 Patient-Derived Xenografts (PDXs), carrying EGFR L858R and *CDK6* amplification, treated with vehicle, palbociclib (150 mg/Kg) or osimertinib (5 mg/Kg); normalized quantification of the level of p-EGFR versus the expression of the total mutant protein is provided in the lower bar-plot. (B-C) Growth curves (B) and percentage of tumor volume change (C) for TH116 Patient-Derived Xenografts (PDXs), carrying EGFR L858R and *CDK6* amplification treated with vehicle, osimertinib (5 mg/Kg), palbociclib (100 mg/Kg) or combination of osimertinib and palbociclib (Osi. + Palbo.) (n = 7 xenografts per group; ***$P < 0.001$, *$P < 0.05$). (D) Growth rate of TH116 PDXs treated with osimertinib (5 mg/Kg) or combination of osimertinib (5 mg/Kg) and palbociclib (100 mg/Kg, Osi. + Palbo.) (*$P = 0.01$, Student's t-test). (E-F) Representative hematoxylin/eosin and γH2AX IHC stain images (E) and quantification (F) using tissues from TH116 PDXs (n = 4 xenografts per group; **$P < 0.01$, Student T-test). (G) FGA analysis in TH116 PDXs, treated with vehicle, osimertinib (5 mg/Kg), palbociclib (100 mg/Kg) or combination of osimertinib and palbociclib (Osi. + Palbo.) (*$P = 0.001$, n = 2 xenografts per group).

(Veh.: vehicle; Palbo.: palbociclib; Osi.: osimertinib; p-value assessed by one-way Anova and Tukey's multiple comparisons test; error bars representing SEM).
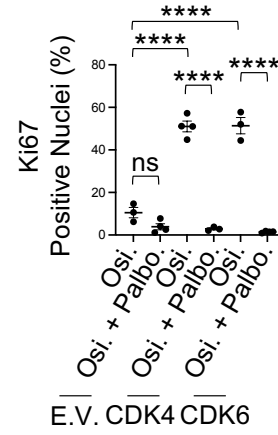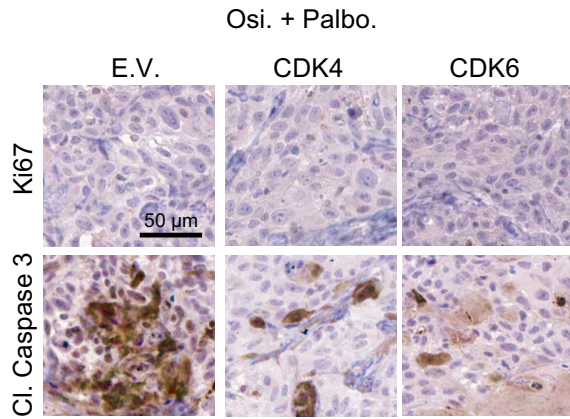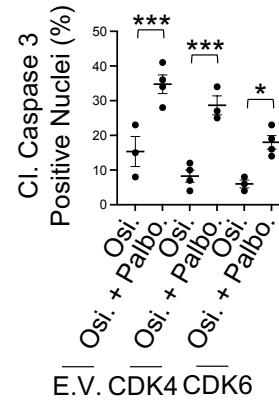
See also Supplementary Figure 15.

Figure 8

A

H1975 CDXs

Osimertinib

E.V.   CDK4   CDK6

Ki67

Cl. Caspase 3

50 µm

C

Ki67
Positive Nuclei (%)

ns   ****   ****   ****

E.V. CDK4 CDK6

Osi.
Osi. + Palbo.

B

Osi. + Palbo.

E.V.   CDK4   CDK6

Ki67

Cl. Caspase 3

50 µm

D

Cl. Caspase 3
Positive Nuclei (%)

***   ***   *

E.V. CDK4 CDK6

Osi.
Osi. + Palbo.

E

CDK4/6 wt
CCND1

Rb1
E2F

EGFR signaling off
Osimertinib

nucleus

CCNE1

Proliferative arrest
Apoptosis

EGFR TKI sensitive
Proliferation arrest and apoptosis

F

CDK4/6 amp
CCND1

Rb1
E2F

P P P Rb1 P

E2F   CCNE1

EGFR signaling off
Osimertinib

nucleus

Proliferation

RS GIN

TPX2 ATM

Survival

Resistance
SNVs
CNAs

EGFR TKI resistant
Proliferation and survival

G

CDK4/6 amp
CCND1

CDK4/6i

Rb1
E2F

CCNE1

EGFR signaling off
Osimertinib

nucleus

Proliferative arrest
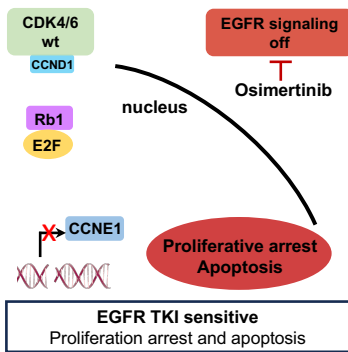Apoptosis
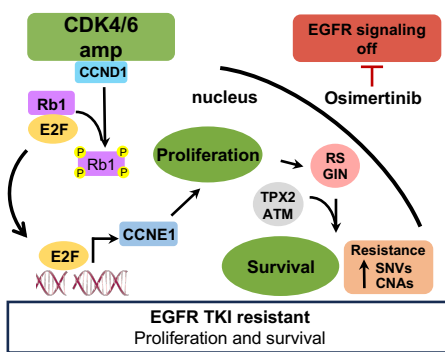
EGFR TKI sensitive
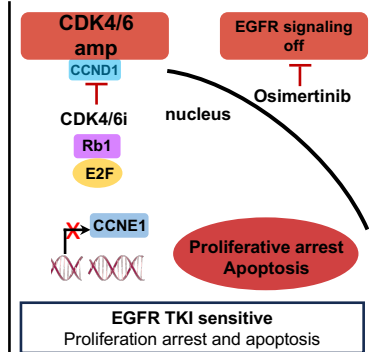Proliferation arrest and apoptosis

46

Figure 8 - Combination therapy with EGFR and CDK4/6 inhibitors suppresses tumor proliferation and increases apoptosis in CDK4/6 o/e EGFRmt CDXs.

(A-D) Representative IHC stain images (A-B) and quantification (C-D) of Ki67 (A-B top panels) and cleaved caspase 3 (A-B bottom panels) using tissues from E.V. and CDK4/6 overexpressing H1975 CDXs treated with osimertinib (5 mg/Kg) in mono- (A) or combinatorial (B) treatments with palbociclib (100 mg/Kg) (n = 3-4 xenografts per group; E.V.: empty vector; CDK4: CDK4 overexpressing CDXs; CDK6: CDK6 overexpressing CDXs; Osi.: osimertinib; Osi. + Palbo.: osimertinib + palbociclib; ****P < 0.0001, ***P < 0.001, **P < 0.01, *P < 0.05; p-value assessed by one-way Anova and Tukey's multiple comparisons test; error bars representing SEM). (E-G) Model showing the effects of CDK4/6 AMP in EGFRmt LUAD: in the setting of *CDK4/6* wild type, EGFR TKI treatment induces proliferation arrest and apoptosis (E). In the setting of *CDK4/6 AMP*, Rb phosphorylation is maintained and EGFR TKI treatment is not able to induce growth arrest (F). Tumor proliferation continues with accumulation of RS, GIN and activation of TPX2/AURKA and DDR protective mechanisms, which leads to accumulation of gene SNVs (e.g. SNVs belonging to TGF-β, NRF2, RTK/RAS and WNT pathways) and CNAs (e.g. *EGFR*, *CDK6, MET*, *BRAF* copy number gains) contributing to EGFR TKI resistance (F). The addition of a CDK4/6 inhibitor to EGFR TKI treatment blocks Rb phosphorylation and maintains Rb expression leading to G1/S arrest allowing cells with accumulated GIN to undergo apoptosis and cell death (G). The subsequent decrease in tumor cell proliferation and increase in cell death of tumor cells with GIN results in tumor karyotype selection and growth arrest (RS: Replication Stress; GIN: Genomic Instability; DDR: DNA Damage Response pathway; CNAs: Copy Number Alterations; SNVs: Single Nucleotide Variants).